Large Area 3D Elemental Mapping of a MgZnO/CdTe Solar Cell with Correlative EBSD Measurements

Thomas A. M. Fiducia[1], Kexue Li[2], Amit H. Munshi[3], Kurt Barth[3], Walajabad S. Sampath[3], Chris Grovenor[2], and John M. Walls[1]

[1]Loughborough University, Loughborough, Leicestershire, LE11 3TU, United Kingdom,
[2]Materials Department, Oxford University, Oxford, OX1 3PH, United Kingdom
[3]Colorado State University, Fort Collins, Colorado, 80523, USA

***Abstract* — Chlorine is known to have numerous effects on the electronic performance of cadmium telluride (CdTe) solar cells, such as doping the CdTe absorber material and pacifying crystal defects. However the mechanisms by which the element improves device efficiency following the cadmium chloride treatment are still not fully understood. In this work the distributions of chlorine in a high efficiency CdTe device are tracked over large areas and in three dimensions by high resolution dynamic SIMS measurements. The results give new insights into the role of chlorine and defects on the performance of CdTe solar cells, particularly when combined with correlative backscatter diffraction measurements.**

***Index Terms* — $CdCl_2$, CdTe, Chlorine, defects, EBSD, SIMS, twin boundary.**

I. Introduction

In the last seven years the record cadmium telluride (CdTe) solar cell efficiency has risen from ~16% to 21.0% [1], [2]. However cell voltages need to improve for CdTe to approach its single junction efficiency limit of around 30% [3], [4]. While device simulations have shown that this can be achieved by simultaneously improving carrier lifetimes and carrier concentrations, non-radiative carrier recombination at crystal defects in the material currently limits lifetimes and hence cell voltages [5].

The ubiquitous cadmium chloride ($CdCl_2$) heat treatment is known to help in this regard, as chlorine that enters the device pacifies grain boundaries to some extent [6]. However the treatment – which takes devices from a maximum of a few percent efficiency, up the typical values seen of over 10% – causes a myriad of other microstructural and chemical changes in the device. It is therefore difficult to discern which are the most important in improving efficiency. The changes include a reduction in the density of stacking faults and twins in the grain interiors, inter-diffusion of sulphur from the cadmium sulphide (CdS) layer into the CdTe (in CdS/CdTe devices), and insertion of chlorine into grain interiors and at the front interface [7]–[9]. In this work the distributions of chlorine, tellurium, oxygen, magnesium and zinc in a MgZnO/CdTe device are mapped in 3D by high resolution dynamic SIMS to further investigate the role of these elements in improving efficiencies following the cadmium chloride treatment. The study is large area and passes through the depth of the cell, and involves correlative microstructural measurements to aid data interpretation.

II. Experimental

A high efficiency MgZnO/CdTe device was fabricated by Close Space Sublimation (CSS) at Colorado State University [10]. To make the cell, a 100 nm $Mg_{0.23}Zn_{0.77}O$ (MZO) buffer layer was first deposited onto a TEC 10 TCO-coated glass substrate by magnetron sputtering. This was followed by ~4 μm of CdTe deposited by CSS, resulting in the device structure shown in Fig 1. The stack was then exposed to a cadmium chloride activation treatment lasting six minutes and a copper chloride doping treatment. Finally, the cell was contacted with a layer of nickel-carbon paint. The cell was measured at 15.0% efficiency under a standard AM 1.5 spectrum. To prepare the cell for further characterisation a region of the CdTe back surface was polished with a gallium Focused Ion Beam (FIB) to remove surface roughness (see schematic in Fig 1).

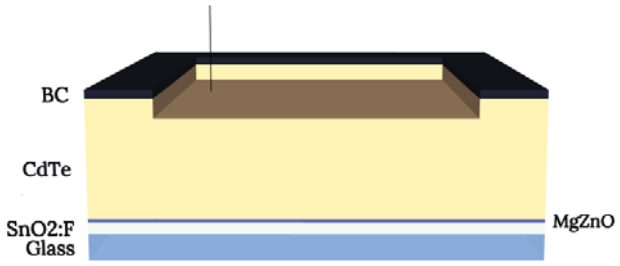

Fig. 1 Schematic of the device structure and polished back surface on which the SIMS was performed. Layer thicknesses are to scale apart from the glass and back contact (Glass 3 mm, SnO_2 400 nm, MgZnO 100 nm, CdTe 4 μm, back contact 25μm).

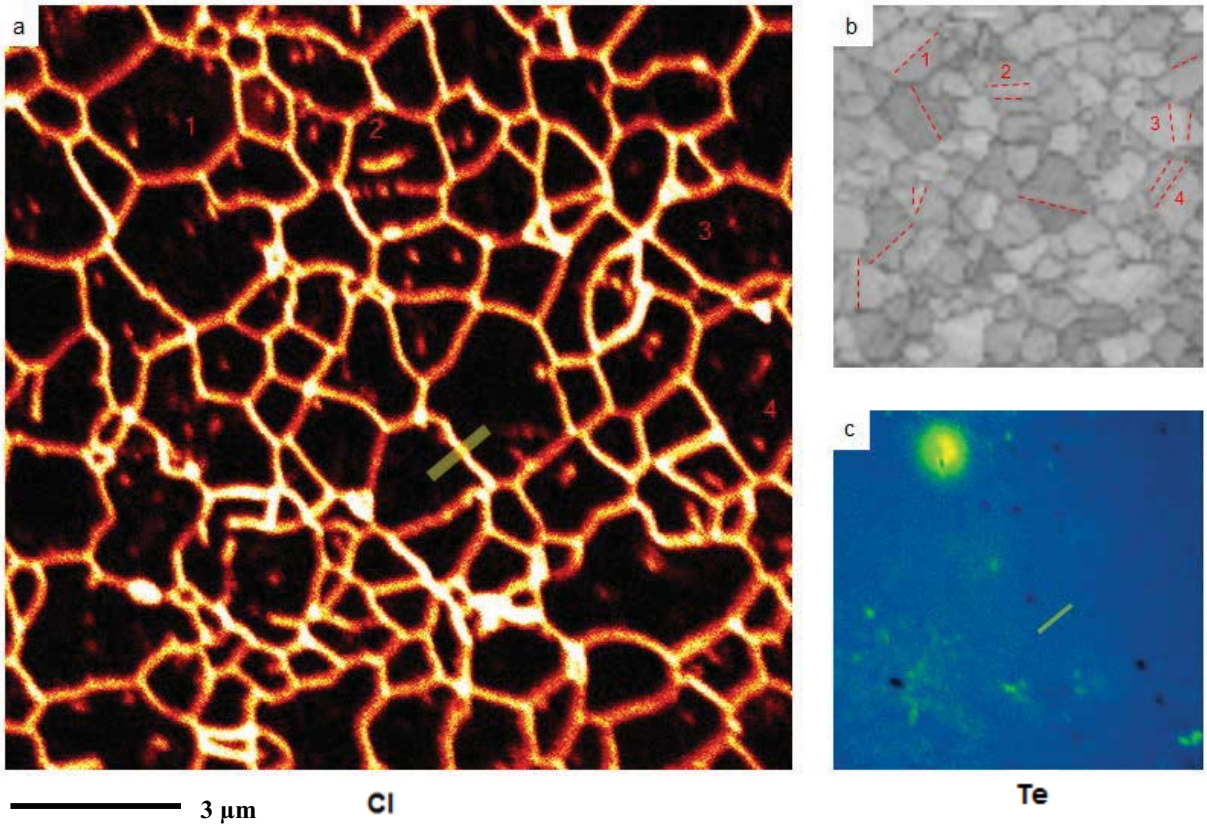

Fig. 2 (a) Chlorine intensity map taken at the back of the CdTe. The yellow annotation shows where the line profile in Fig 3 (c) was taken. (b) EBSD band contrast map of the same region in (a). A selection of Σ3 (111) twin boundaries are highlighted in red. Numbers 1 – 4 show the equivalent grains in (a). (c) Te map of the same region shown in (a) and (b). The yellow annotation shows where the line profile in Fig 3 (c) was taken.

Following the Ga ion polish, Electron Back-Scatter Diffraction (EBSD) was performed on a 20 x 20 μm region on the surface of the cell. This provides information on grain orientations and therefore grain boundary types in the analysed area.

Correlative high-resolution SIMS measurements were then taken on the same area with a Cameca 50/50L NanoSIMS. During the measurements a 0.5-1 pA Cs^+ ion beam with a nominal diameter of 60 nm was rastered over the surface and sputtered secondary ions were analysed with a double-focused mass spectrometer. Masses analysed were $^{35}Cl^-$, $^{130}Te^-$, $^{24}Mg^{16}O^-$, $^{64}Zn^{16}O^-$, and $^{16}O^-$, and so a high-resolution map of each of these elements is formed following the raster (MgO and ZnO are used instead of Mg and Zn as the oxides are negatively charged and therefore detectable by the NanoSIMS). On repeating the process a 3D data cube is built up of elemental distributions in the analysed volume.

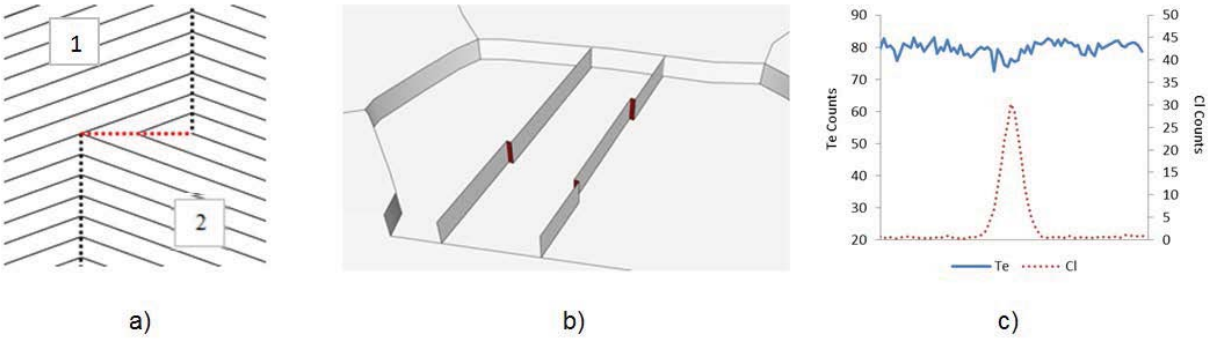

Fig. 3 (a) Schematic of a kink in a Σ3 (111) lamellar twin boundary forming a Σ3 (112) double-positioning twin boundary (vertical dotted lines and horizontal red dotted line respectively). The <111> direction points vertically up the page. (b) Schematic of kinks in Σ3 (111) twins in the setting of a grain. (c) Line profile of the chlorine and tellurium counts in the regions shown in Fig. 2 (a) and (c).

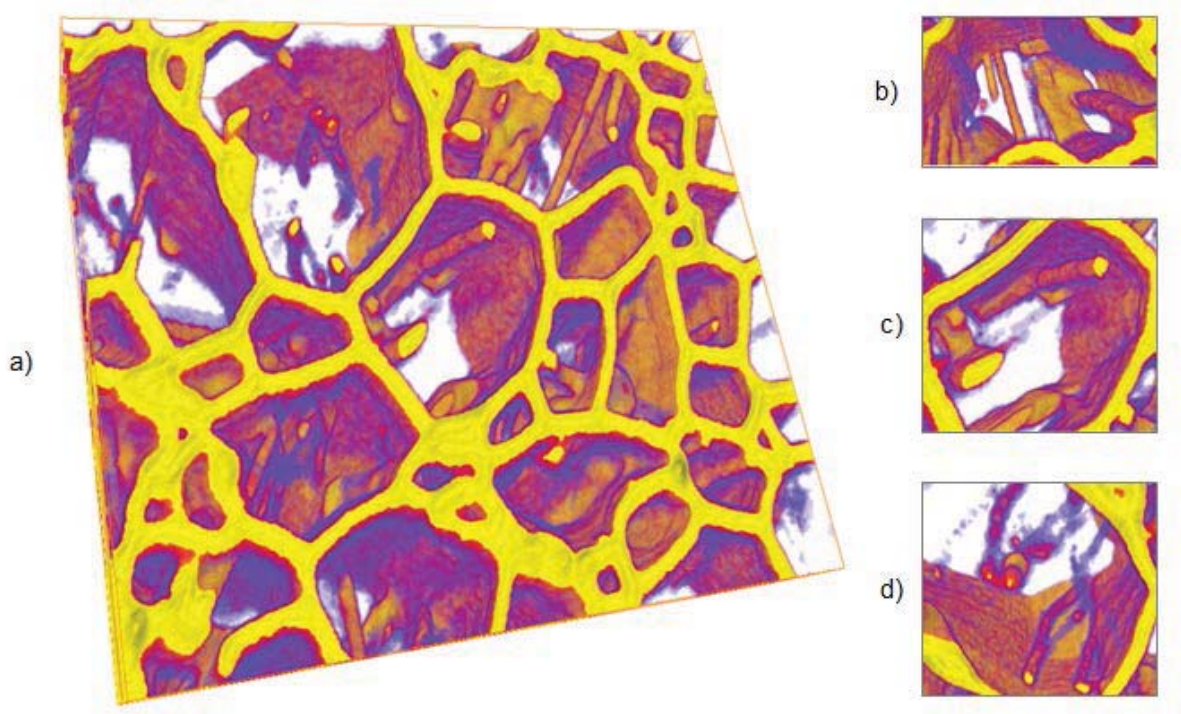

Fig. 4 (a) 3D rendering of the chlorine signal in the CdTe absorber layer (different region from map in Fig. 2). Area 8.3 μm x 7.4 μm. (b-d) Re-oriented and close-up views of linear chlorine features in the grain interiors.

III. Results

Fig. 2 (a) shows a chlorine intensity map of a region on the back surface of the CdTe. Apart from the Cl signal network at the grain boundaries there are numerous signal hot spots in the grain interiors. Part (c) of the figure shows that the hot spots do not correspond to fluctuations in the Te signal. However, the EBSD imaging performed on the same region prior to the SIMS measurement reveals that the spots often occur along $\Sigma 3$ (111) twin boundaries – lamellar twins. This can be seen by comparison of the Cl map to the EBSD map in part (b) of the figure, which has had a selection of lamellar twins highlighted. For example, hot spots in grains 1, 2, 3 and 4 clearly lie on twins in those grains (it is also worth noting that there is often more than one chlorine hot spot along a single twin boundary in a grain). Spots occur at a density of around one per 2.9 μm^2, and careful inspection of the data reveals that around one third of these can be directly associated with a lamellar twin boundary (it may be that more are associated, but higher resolution EBSD would be needed to show it clearly). Tomographic SIMS shows that in three dimensions the hot spots form rod-shaped features in the chlorine signal that generally span grains. This can be seen in the 3D renderings of the chlorine signal in figure 4 (a – d). The close-up in part (c) of figure 4 shows two rod-shaped GI chlorine features that lie in the same plane, and part (d) shows two separate instances of a pair of linear chlorine features lying in the same plane.

Another feature that is apparent from Fig. 2 is that there are faint lines of lower signal in the tellurium map. These can be mapped directly onto the grain boundary network seen in Fig 2 (a). In addition the line profile in Fig 3 (c) shows a dip in the tellurium signal at the point where the chlorine signal rises at the boundary. In this case the drop in the tellurium counts is between 5-10%, and this is typical for the boundaries seen in the Te map.

The 3D nature of the SIMS means that behaviour of elements through the depth of the cell can be tracked. Figure 5 shows reconstructed cross sectional images of the chlorine, oxygen, magnesium and zinc signals. A layer of chlorine signal is seen at the front interface of the cell, between the CdTe and the MZO. It can be seen that there is a thin region of oxygen signal extending around 500-600 nm into the CdTe layer. However, no magnesium or zinc signal is present in the CdTe.

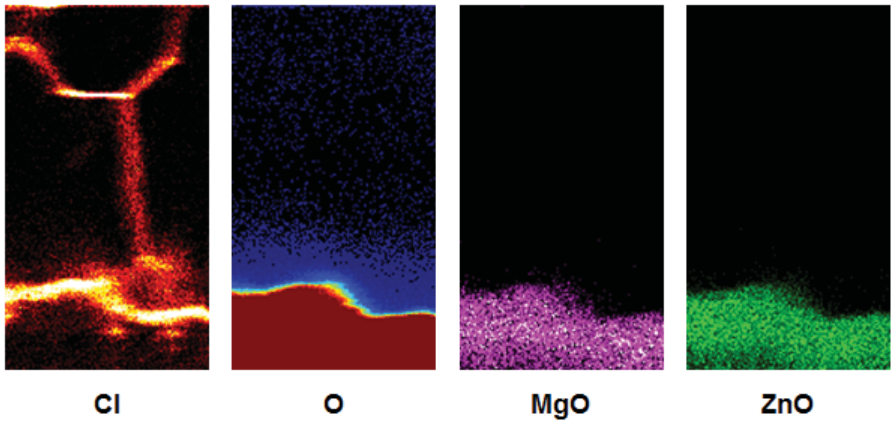

Fig. 5 Cross sectional images of the $^{35}Cl^-$, $^{16}O^-$, $^{24}Mg^{16}O^-$, and $^{64}Zn^{16}O^-$ signals across the front interface of the MZO/CdTe device. In general brighter means higher signal. In the oxygen map red is high intensity and blue is low.

IV. Discussion

The 3D and correlative nature of the measurements, performed over a large area, means that they provide fresh insights into the microstructure and chemistry of the MZO/CdTe cell. For instance, that the hot spots in the chlorine signal are frequently seen to lie along Σ3 (111) lamellar twin boundaries suggests that they are due to chlorine segregation at small kinks in the (111) twins. These kinks would form thin ribbon-shaped features connecting misaligned (111) twins, as shown schematically in figure 3 (b). The linear nature of these defects is consistent with the chlorine signal seen in the NanoSIMS. In addition, the kinks would tend to span the grain, which is again consistent with the SIMS data.

Kinks in lamellar twin boundaries form incoherent twins, a common example of which is the Σ3 (112) 'double positioning' (DP) twin boundary, shown schematically in Fig 3 (a). Twins form between two crystals whose orientations are closely related. In Σ3 twin boundaries they are related by a 180 degree rotation around the <111> direction (see grains 1 and 2 in the schematic). In Σ3 twins 1/3rd of atomic sites are identical in both crystals; hence boundaries between 2 crystals like this are CSL Σ3 twin boundaries in the CSL convention). When the boundary between the two crystals lies on the (111) plane in both the crystals – such as in the vertical dotted boundaries in Fig. 3 (a) – it is called a Σ3 (111) lamellar twin boundary. At these boundaries there is little disruption of the atomic structure across the interface and tetrahedral bonding is maintained. As such Σ3 (111) twin boundaries are thought to be electrically benign [11]. However, when the boundary lies on another crystal plane between the two CSL grains – such as the (112) plane shown in the figure by the horizontal red dotted line - there must be non-tetrahedral bonding at the boundary and it is potentially electrically active. Modelling performed on supercells containing a proposed atomic structure for the Σ3 (112) DP twin has suggested that the defect introduces mid-gap states into the material [12]. It is therefore likely that unpacified Double Positioning twin boundaries are non-radiative recombination centres. However as the SIMS measurements have shown, their open atomic structure means that chlorine can enter the defects. This would be expected to pacify the defects to some extent as it does with random GBs (cathodoluminescence measurements have shown that chlorine improves the electrical properties of general GBs but that they remain non-radiative recombination centres [6], [13]). Combined with the high density of the defects in the material and their position in the centre of grains, this means that incoherent twins are probably influencing device performance. In addition, in untreated devices, the twin and stacking fault density is much higher than in treated material, meaning that the density of twin and SF *terminations* will also be higher. The defects in untreated devices will also be unpacified. The reduction in density and passivation of incoherent and higher order twins during the $CdCl_2$ treatment is therefore another reason for efficiency improvement following treatment.

The 3D SIMS measurements also show that there is a build-up of chlorine at the front interface of the device, where it would be expected to pacify mid-level defects as it does for grain boundaries. In contrast to cells with a CdS buffer layer chlorine does not appear to enter the MZO in significant concentrations [9]. Importantly, no magnesium or zinc is seen to move into the CdTe, but a thin layer of oxygen does move into the absorber. The slight dip in tellurium signal at the grain boundaries suggests that chlorine is to some extent substitutional with the Te, rather than purely interstitial. This is in line with previous work employing STEM EDX and Electron Energy Loss Spectroscopy mapping [14].

IV. Conclusions

High resolution 3D SIMS measurements and correlative EBSD has been performed on a MZO/CdTe solar cell. A large density of chlorine hot spots (forming rods in three dimensions) are found to be present in grain interiors in the cell. Their location along the line of Σ3 (111) lamellar twin boundaries suggests that the spots are due to chlorine segregation at kinks in the twins, i.e. incoherent twin boundaries like the Σ3 (112). Passivation and reduction in density of these defects is therefore likely to be a reason for device efficiency improvements following $CdCl_2$ heat treatment – alongside other known effects like general GB passivation. In addition, the remaining incoherent twins will still be harming device efficiency, and so further reductions in defect density would be a worthwhile goal in CdTe device processing. Finally, neither magnesium nor zinc is found to diffuse into the CdTe layer from the MZO, however a small amount of oxygen is detected in the CdTe.

Acknowledgements

The authors at CSU are thankful for funding support from NSFs Accelerating Innovation Research and NSFs Industry/University Cooperative Research Center programs.

References

[1] M. Gloeckler, I. Sankin, and Z. Zhao, "CdTe Solar Cells at the Threshold to 20% Efficiency," *IEEE J. Photovoltaics*, vol. 3, no. 4, pp. 1389–1393, Oct. 2013.

[2] M. A. Green, K. Emery, Y. Hishikawa, W. Warta, and E. D. Dunlop, "Solar cell efficiency tables (version 46)," *Prog. Photovoltaics Res. Appl.*, vol. 23, no. 7, pp. 805–812, Jul. 2015.

[3] R. M. Geisthardt, M. Topic, and J. R. Sites, "Status and Potential of CdTe Solar-Cell Efficiency," *IEEE J. Photovoltaics*, vol. 5, no. 4, pp. 1217–1221, 2015.

[4] W. Shockley and H. J. Queisser, "Detailed Balance Limit of Efficiency of p-n Junction Solar Cells," *J. Appl. Phys.*, vol. 32, no. 3, p. 510, 1961.

[5] J. M. Burst, J. N. Duenow, D. S. Albin, E. Colegrove, M. O. Reese, J. a. Aguiar, C.-S. Jiang, M. K. Patel, M. M. Al-Jassim, D. Kuciauskas, S. Swain, T. Ablekim, K. G. Lynn, and W. K. Metzger, "CdTe solar cells with open-circuit voltage greater than 1 V," *Nat. Energy*, vol. 1, no. February, p. in press, 2016.

[6] J. Moseley, W. K. Metzger, H. R. Moutinho, N. Paudel, H. L. Guthrey, Y. Yan, R. K. Ahrenkiel, and M. M. Al-jassim, "Recombination by grain-boundary type in CdTe," *J. Appl. Phys.*, vol. 118, 2015.

[7] A. Abbas, G. D. West, J. W. Bowers, P. Isherwood, P. M. Kaminski, B. Maniscalco, P. Rowley, J. M. Walls, K. Barricklow, W. S. Sampath, and K. L. Barth, "The effect of cadmium chloride treatment on close-spaced sublimated cadmium telluride thin-film solar cells," *IEEE J. Photovoltaics*, vol. 3, no. 4, pp. 1361–1366, 2013.

[8] T. Fiducia, A. Abbas, K. Barth, W. Sampath, and M. Walls, "Intragranular Defects in As-Deposited and Cadmium Chloride-Treated Polycrystalline Cadmium Telluride Solar Cells," in *2016 IEEE 43rd Photovoltaic Specialist Conference (PVSC)*, 2016.

[9] T. Fiducia, K. Li, A. Munshi, C. Grovenor, K. Barth, W. Sampath, and J M. Walls, "3D Distributions of Chlorine and Sulphur Impurities in a Thin-Film Cadmium Telluride Solar Cell," 2018. In preparation

[10] D. E. Swanson, J. M. Kephart, P. S. Kobyakov, K. Walters, K. C. Cameron, K. L. Barth, W. S. Sampath, J. Drayton, and J. R. Sites, "Single vacuum chamber with multiple close space sublimation sources to fabricate CdTe solar cells," *J. Vac. Sci. Technol. A Vacuum, Surfaces, Film.*, vol. 34, no. 2, p. 21202, 2016.

[11] S. Yoo, K. T. Butler, A. Soon, A. Abbas, J. M. Walls, and A. Walsh, "Identification of critical stacking faults in thin-film CdTe solar cells," *Appl. Phys. Lett.*, vol. 105, no. 6, p. 62104, Aug. 2014.

[12] Y. Yan, M. M. Al-Jassim, and K. M. Jones, "Structure and effects of double-positioning twin boundaries in CdTe," *J. Appl. Phys.*, vol. 94, no. 5, pp. 2976–2979, 2003.

[13] Y. Yan, M. M. Al-Jassim, and K. M. Jones, "Passivation of double-positioning twin boundaries in CdTe," *J. Appl. Phys.*, vol. 96, no. 1, pp. 320–326, 2004.

[14] C. Li, J. Poplawsky, Y. Yan, and S. J. Pennycook, "Understanding individual defects in CdTe thin-film solar cells via STEM: From atomic structure to electrical activity," *Mater. Sci. Semicond. Process.*, vol. 65, no. June 2017, pp. 64–76, 2016.